https://doi.org/10.5194/nhess-2019-207
Preprint. Discussion started: 2 July 2019

Natural Hazards and Earth System Sciences
Discussions

Modelling Global Tropical Cyclone Wind Footprints

James M. Done[1,2], Ming Ge[1], Greg J. Holland[1,2], Ioana Dima-West[3], Samuel Phibbs[3], Geoffrey R. Saville[3], and Yuqing Wang[4]

[1]National Center for Atmospheric Research, 3090 Center Green Drive, Boulder CO 80301, US
[2]Willis Research Network, 51 Lime St, London, EC3M 7DQ, UK
[3]Willis Towers Watson, 51 Lime St, London, EC3M 7DQ, UK
[4]International Pacific Research Center and Department of Atmospheric Sciences, School of Ocean and Earth Science and Technology, University of Hawaii at Manoa, HI 96822, US.

Correspondence to: James M. Done (done@ucar.edu)

Abstract. A novel approach to modelling the surface wind field of landfalling tropical cyclones (TCs) is presented. The modelling system simulates the evolution of the low-level wind fields of landfalling TCs, accounting for terrain effects. A two-step process models the gradient-level wind field using a parametric wind field model fitted to TC track data, then brings the winds down to the surface using a full numerical boundary layer model. The physical wind response to variable surface drag and terrain height produces substantial local modifications to the smooth wind field provided by the parametric wind profile model. For a set of U.S. historical landfalling TCs the simulated footprints compare favourably with surface station observations. The model is applicable from single event simulation to the generation of global catalogues. One application demonstrated here is the creation of a dataset of 714 global historical TC overland wind footprints. A preliminary analysis of this dataset shows regional variability in the inland wind speed decay rates and evidence of a strong influence of regional orography. This dataset can be used to advance our understanding of overland wind risk in regions of complex terrain and support wind risk assessments in regions of sparse historical data.

1 Introduction

Tropical Cyclones (TCs) dominate U.S. weather and climate losses (Pielke Jr., et al. 2008; Smith and Katz, 2013). They account for 41% of the inflation-adjusted U.S. insured loss between 1995 and 2014. Future increases in TC peak wind speeds (Walsh et al., 2016), in combination with rapid population increases, mean TC wind losses are set to rise even further (Geiger et al., 2016; Estrada et al., 2015; Ranson et al., 2014; Weinkle et al., 2012). Improved approaches to assessing overland TC wind fields is needed to enable society to manage this increasing risk.

While coastal communities may experience relatively frequent TC impacts, inland communities experience TC impacts far less often and less is known about the likelihood of inland damaging winds. Given the scientific consensus that average TC wind speeds will increase in the future (e.g., Villarini and Vecchi, 2013; Murakami et al., 2012; Hill and Lackmann, 2011;

https://doi.org/10.5194/nhess-2019-207
Preprint. Discussion started: 2 July 2019


Natural Hazards and Earth System Sciences Discussions

Elsner et al., 2008) and that category 4 and 5 hurricanes have increased substantially in recent decades (Holland and Bruyère, 2014), strong winds may be experienced farther inland in the future, all other TC and environment characteristics being equal. Modelling approaches the capture TC footprints - the entire overland storm-lifetime maximum wind speed from the immediate coast to far inland - is therefore a key need.

New views of global TC footprints are critically needed to support a variety of risk management techniques across a range of timescales. At short timescales, in the immediate few days ahead of a landfalling TC, what is the physically credible range of footprint scenarios, and thus potential losses? At longer timescales, what is the impact of coastal terrain features on TC wind distributions and potential losses? And how does terrain affect overland extreme wind probabilities? Long records of TC overland wind footprints are also critically needed to appraise traditional modelling approaches, inform the generation of synthetic event sets (particularly in regions of sparse historical data), and to inform near- and long-term views of wind probability accounting for climate variability and incorporating the effects of climate change. Historical event footprints can be used to better understand historical losses, and to create physically plausible worst-case TC scenarios, known as realistic disaster scenarios in the re/insurance industry. A global catalogue of TC wind footprints is also needed to advance our basic understanding of TC climate across basins. For example, what are the global- to local-scale processes controlling regional spatial and temporal trends and variability of overland TC winds?

Using an analytical boundary layer model to simulate the low-level winds during Hurricane Fabian (2003) over Bermuda, Miller et al., (2013) found winds at the crest of a ridgeline at category 4 strength compared to category 2 strength in simulations without terrain. Simulations of Cyclone Larry (2006) over the coastal ranges of Queensland, Australia using a full numerical weather prediction model by Ramsay and Leslie (2008) also produced wind speed-ups along hill crests and windward slopes. The high Froude number flow brought about by the high wind speeds and quasi-neutral stability causes flow directly over the terrain features with minimal lateral displacement. Under mass continuity, the flow accelerates as the air column thins passing over higher terrain. This speed-up also supports wind-shear driven turbulence and enhances peak gusts.

Given that the work done by the wind in directly damaging structures varies by the cube of the wind speed (Emanuel, 2005), terrain effects on damage have the potential to be significant. Indeed, Miller et al., (2013) found that the greatest residential roof damage was located along the ridgeline and the windward slopes of Bermuda. Terrain effects were also found in residential wind damage patterns during Cyclone Larry in 2006 (Henderson et al., 2006) and during Hurricane Marilyn in 1995 across the Island of St Thomas in the Caribbean (Powell and Houston, 1998). Incorporating terrain effects could therefore improve wind risk assessments when compared to traditional analytic methods in regions of complex terrain, thus supporting potential losses assessments and underwriting decisions in re/insurance markets.

Current practice in surface wind field modelling spans a range of complexity, depending on the application. The simplest

https://doi.org/10.5194/nhess-2019-207
Preprint. Discussion started: 2 July 2019


Natural Hazards and Earth System Sciences Discussions

models, known as parametric radial wind profiles (e.g., Holland et al., 2010; Willoughby et al., 2006), fit functions to a small number of readily available TC and environmental parameters to characterize the radial profile of surface wind and pressure from the TC centre. They are computationally efficient and therefore widely used as the hazard component of catastrophe models (Mitchell-Wallace et al., 2017; Vickery et al., 2009), and can be used to compute wind exceedance probabilities anywhere on Earth. But fast computation comes at a price. The resulting wind fields are smooth, and so empirical corrections are typically applied to represent surface terrain effects.

An alternative approach is a reanalysis of observations. A reanalysis is created using a physical model that is nudged towards available observations. While a reanalysis produces gridded data and may capture observed asymmetries, it may still miss the effects of a variable surface roughness [e.g., HWIND (Powell et al., 1998) is representative only of open terrain], and to date only a small fraction of historical global events has been reanalysed. Another alternative approach is geostatistical spatial modelling. This data-driven approach combines spatial statistics to capture spatial dependence with extreme value theory to capture peak wind speeds. Again, this model is highly efficient but so far has only been developed for European windstorms (Youngman and Stephenson, 2016) to the authors' knowledge. Finally, four-dimensional high-resolution numerical modelling captures many more physical processes (e.g., Davis et al., 2010). But it is computationally too expensive and can be used only in a small number of cases. It is therefore of marginal use as the hazard component of catastrophe models, aside from use to develop improved parametric models (Loridan et al., 2015; Loridan et al., 2017).

This paper describes a novel and globally applicable approach to modelling the surface wind field of landfalling TCs. The model was developed as a collaboration between atmospheric scientists and reinsurance industry experts to ensure the model and resulting datasets are readily applicable to decision-making processes and based in peer-reviewed science. The modelling system combines the high efficiency of the parametric profile model with a representation of the interaction of the flow and variable surface terrain that captures the essential dynamics and physics. The modelling system simulates the temporal evolution of the near-surface spatial wind fields of landfalling TCs, accounting for terrain effects such as coastal hills and abrupt changes in surface roughness due to coastlines, forested or urban areas. The approach fits a parametric wind field model to historical or synthetic TC track data, and captures the frictional response of the wind field to the Earth's surface using a 3-dimensional numerical model of the lowest 2-3km of the atmosphere.

Application of the model is demonstrated through the creation of a dataset of 714 historical landfalling TC footprints globally. Such global footprint datasets have been created before but none used a non-linear boundary layer model that captures the dynamical response to a variable lower boundary. Giuliani and Peduzzi (2011) utilized a dataset of global historical TC footprints generated using a parametric model. More recently, Tan and Fang (2018) generated a dataset of 5376 global historical footprints using an approach that simulates the gradient winds using a parametric wind profile model and bringing the winds down to the surface using a simple power law profile that depends on the local surface roughness (Meng et al.,

https://doi.org/10.5194/nhess-2019-207
Preprint. Discussion started: 2 July 2019


Natural Hazards and Earth System Sciences
Discussions

1997). Terrain effects were included using a simple speed-up factor based on 4 categories of terrain type and wind direction. By using a 3-dimensional model our approach includes additional dynamical effects such as non-linear development.

The next section describes the modelling approach. Section 3 describes the simulation results of selected case studies. A model evaluation against surface station observations is provided in Section 4. Section 5 describes the dataset of global historical landfalling TC footprints and includes a preliminary analysis. Finally, conclusions are presented in Section 6.

2 Method

A TC footprint is generated using a two-stage modelling process bookended by pre- and post-processing steps, as summarized by the flow diagram in Fig. 1. Stage one fits a parametric model of upper winds and pressure to the input TC track data. Stage two applies a 3-dimensional numerical boundary-layer model to generate a detailed surface wind field incorporating the effects of terrain features such as coastlines, inland orography, and variable land surface friction.

The pre-processing step removes an estimate of the asymmetry due to storm motion (V_s) from the maximum wind speed input from the TC track data. The portion removed is a function of the TC translation speed, $V_s=1.173V_t^{0.63}$, following Chavas et al., (2017). The post-processing step then adds back an estimate of the asymmetry due to storm motion to the output surface wind velocity field. The fraction of the storm motion vector added is 1 at the radius of maximum winds and then decays with increasing radius, following Jakobsen and Madsen (2004).

The final footprint is a map of the storm lifetime maximum 1-minute average wind at 10 meters above the Earth's surface. The boundary layer model of Kepert and Wang (2001, hereafter KW01) outputs the instantaneous wind speed at 10 meters above the surface which is the lowest model level. While the instantaneous wind field output from a numerical model does not directly correspond to a specific averaging interval, some guidance is provided by the model timestep. A typical KW01 timestep of 4 seconds adequately resolves variability at timescales of a minute. The footprint is then simply calculated as the storm lifetime maximum wind speed. Frequent model output intervals or a weak smoother may be needed to minimize the appearance of rings of strong winds in the footprint, particularly for fast moving TCs.

https://doi.org/10.5194/nhess-2019-207
Preprint. Discussion started: 2 July 2019

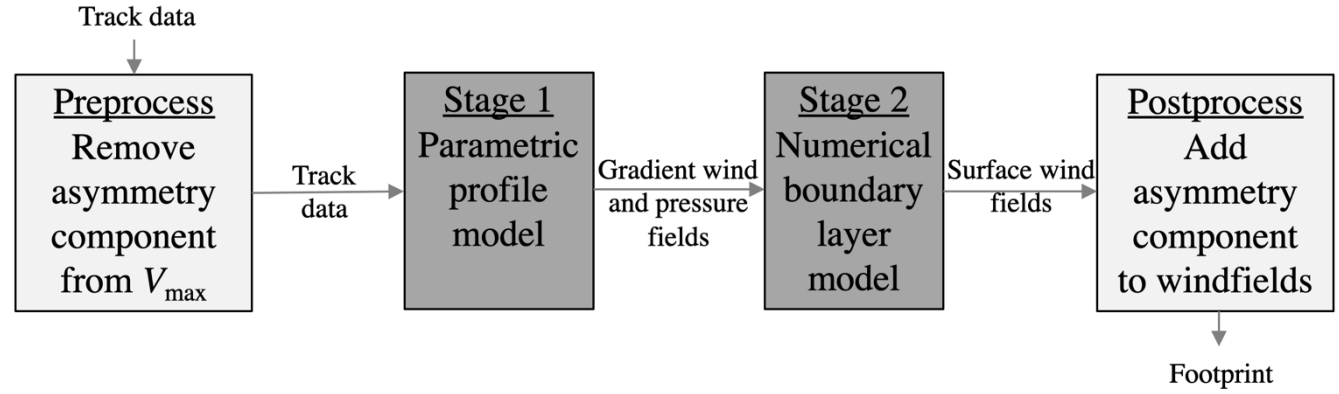

Figure 1: Workflow diagram of the two-stage modelling process, bookended by pre- and postprocessing steps.

2.1 Input Tropical Cyclone Track Data

The model is agnostic to the source of the TC track data. The track may be historical, synthetic or a real-time forecast. Typical historical data sources include the global International Best Track for Climate Stewardship (IBTrACS, Knapp et al., 2010), the Extended Best Track Dataset (Demuth et al., 2006, for the East Pacific and North Atlantic), or from the Joint Typhoon Warning Center (JTWC). Track data require latitude, longitude, maximum wind speed (V_{max}), radius of maximum wind (R_{max}), and environmental pressure. To emphasize the use of only readily available data, we choose to use an average value of R_{max} around the storm. If the Holland et al., (2010) wind profile is used (discussed in the next section), an additional variable of the radius of 34kt winds is required. Sensitivity tests (not shown) found that the model requires new track data every 10 minutes, to smooth out changes in the forcing of KW01 and reduce shocks. These can be obtained by simple interpolation.

2.2 Stage 1: Modelling the Gradient-Level Wind and Pressure Fields

Initial solutions for the gradient-level spatial wind and pressure fields are created for each time step using a parametric profile model. The gradient-level solution represents upper winds unaffected by frictional and terrain effects from the lower surface boundary. For TCs this level is typically between 500m and 1.5km above the surface, depending on definition, and decreasing towards the TC centre (Zhang et al., 2011). Parametric profile models use functional radial profiles to determine the wind speed and pressure field from the TC centre [see Vickery et al., (2009) for an overview]. Our modelling approach is flexibly adaptable to use most choices of radial profile model. Sensitivity tests (not shown) with the Holland et al., (2010) and Willoughby et al., (2006) profiles showed some differences. The Holland et al., (2010) profile has the advantage of tying down the radial decay profile using an observation of an outer wind, say the radius of 34 knot winds. However, observations of outer winds are not readily available globally. Willoughby et al., (2006) uses a sectionally continuous wind-profile comprising a power law inside the eye and two exponential decay functions outside. A polynomial smooths the transition across the radius of maximum wind. This allows greater flexibility for using those databases without 34 kt wind radii. The

https://doi.org/10.5194/nhess-2019-207
Preprint. Discussion started: 2 July 2019


Natural Hazards and Earth System Sciences Discussions

viability of forcing KW01 with the Willoughby profile was demonstrated by Ramsay et al., (2009) for a case study simulation of Tropical Cyclone Larry (2006), by Kepert (2006a) for Hurricane Georges (1998), Kepert (2006b) for Hurricane Mitch (1998), and Schwendike and Kepert (2008) for Hurricanes Danielle (1998) and Isabel (2003). Willoughby et al., (2006) conducted a comprehensive evaluation using flight level data. The fewer required data inputs and the verified performance of Willoughby motivated our choice of Willoughby profile for all simulations presented in this paper. We choose to calculate profile parameters using Eqn. (11) of Willoughby et al., (2006) to capture dependencies on R_{max}.

The Willoughby profile requires V_{max} at gradient wind level. The input track V_{max} is almost universally an estimate of the surface value, so an inflation factor of 1.32 is used to inflate the wind estimate from a surface to a gradient level value. While this represents a tunable parameter in our approach, it was selected based on our sensitivity tests for a few historical events (not shown). These sensitivity tests showed KW01 produced inflation factors for surface-to-gradient level wind speeds ranging from 1.11 to 1.43 around the vortex, which agree well with the mean value of 1.32 obtained from 150 dropsonde observations by Powell et al., (2003).

2.3 Stage 2: Modelling the Atmospheric Boundary Layer

A key advantage of our modelling approach over traditional approaches is the use of a numerical boundary layer model to generate a surface wind field. Winds in the boundary layer, the layer between the gradient wind level and the surface, are modelled using a modified version of KW01. KW01 is initialized with the gradient-level wind and pressure fields from the parametric model throughout the entire depth of the boundary layer. It then uses the dry hydrostatic primitive equations (solving for atmospheric flow under conservation of mass, conservation of momentum and accounting for heat sources and sinks) to spin up a steady state boundary layer wind structure in balance with the gradient winds and pressures. Moisture is excluded from the model because of its negligible effects on boundary layer flow. We selected this non-linear model because of its ability to develop important boundary layer structures such as the super-gradient jet (KW01; Kepert, 2006).

The model rapidly achieves steady state in the strongly forced TC environment characterized by large momentum fluxes and fast adjustments (not shown). The model has 18 vertical levels on a height-based vertical coordinate with the model top fixed at 2.0km. This number of vertical levels is far higher than used in most numerical weather prediction models. While the boundary layer height likely varies substantially across global TCs, we choose to keep this fixed in the absence of readily available data. Sensitivity tests (not shown) show that horizontal grid spacings of 2- to 4km are sufficient to maintain the tight pressure gradients of strong TCs, and to capture the effects of major terrain features such as coastal ranges or coastal urban areas.

The highly turbulent boundary-layer flow is treated using a high order turbulence scheme with prognostic turbulent kinetic energy and turbulence dissipation, following Galperin et al., (1988). The turbulence length scale is diagnostic and is capped

https://doi.org/10.5194/nhess-2019-207
Preprint. Discussion started: 2 July 2019


Natural Hazards and Earth System Sciences Discussions

at 80m following Blackadar, (1962). While the model captures the effects of shear-driven turbulence, it does not represent strong thermal effects such as buoyancy. But these thermal effects are negligible for most TC boundary layers where the Richardson number (the ratio of buoyancy-driven to shear-driven turbulence) is close to zero.

Two code modifications were necessary for the simulation of time-evolving and landfalling TCs. The first allows the boundary layer solution to respond to translating TCs and TCs that change in intensity and/or size. The upper winds and pressure are fixed to the parametric model at each time step, to force the boundary layer winds to keep up with the translating storm. In addition, a translation vector is added to the horizontal advection terms in KW01. The portion of the translation vector added reduces close to the surface due to surface friction. To allow the boundary layer winds to respond to changes in vortex structure, the forcing of the model from the upper winds and pressure field is updated every 10 minutes and interpolated to each time step. While KW01 found 24 hours was needed for the boundary layer to spin up an equilibrium state, running for 24 hours for each forcing update is computationally impractical. Sensitivity tests (not shown) showed that the surface winds, the most important for this study, respond rapidly to changes in the forcing. In addition, the boundary layer solution has a memory through the translating advection terms.

The second modification allows the boundary layer solution to respond to real-world terrain height and surface roughness as the TC tracks over land. Terrain elevation data are provided by the Global Multi-Resolution Terrain Elevation Dataset 2010 at 30 arc-seconds (Danielson and Gesch, 2011), and are interpolated onto the model grid. Terrain height enters the boundary layer model through the computation of vertical diffusion and vertical advection, where higher terrain enhances both. Terrain height is first normalized by the height of the model top and capped at 0.9. Vertical motion is diagnosed through the 3-dimensional continuity equation integrating upwards given terrain height and horizontal velocity. Mass may therefore enter or exit the model top according to the requirement to balance net horizontal convergence. Land-use roughness is provided by the MODIS-based 21 category land use data at 30 arc-seconds. The model feels the variable surface roughness through the drag coefficient term. Over land a neutral drag coefficient depends on the surface roughness (Garrett, 1977). Over the ocean, the Charnock relation modified by Smith (1988) is used to account for the effects of increased roughness as wave heights grow with wind speed.

3 Results

A series of simulations of increasingly model complexity is presented here to illustrate the importance of variable land surface friction and orography. Using the case study of Hurricane Maria (2017) over Puerto Rico we compare simulations using i) the Willoughby profile only, ii) the Willoughby profile and KW01 but without land, and iii) the Willoughby profile and KW01 with land. All simulations were run at 2km grid spacing. Figure 2 compares the three footprints. Figure 2a shows that the Willoughby profile captures the decaying winds as Maria crossed Puerto Rico but misses any abrupt changes in the onshore and offshore flow, as expected. In the absence of changing surface friction and terrain at landfall, the only information the

https://doi.org/10.5194/nhess-2019-207
Preprint. Discussion started: 2 July 2019

Natural Hazards and Earth System Sciences
Discussions

model has about landfall is through the decreasing V_{max} in the input track data. The addition of the boundary layer model brings an overall reduction of the footprint (Fig. 2b) by approximately 10% as KW01 responds to the effects of surface friction of the sea surface, as expected. Maximum values of the footprint in the vicinity of the track agree well with the input track V_{max} values (shown by the coloured dots along the track). Finally, the addition of land including variable surface roughness and terrain height (Fig. 2c) causes much greater small-scale variability in the footprint over land. Variable terrain height results in wind acceleration on windward slopes and mountain crests. Variable surface roughness results in sharp transitions in the wind speed along coastlines and, for example, over the urban area of San Juan in the northeast of mainland Puerto Rico.

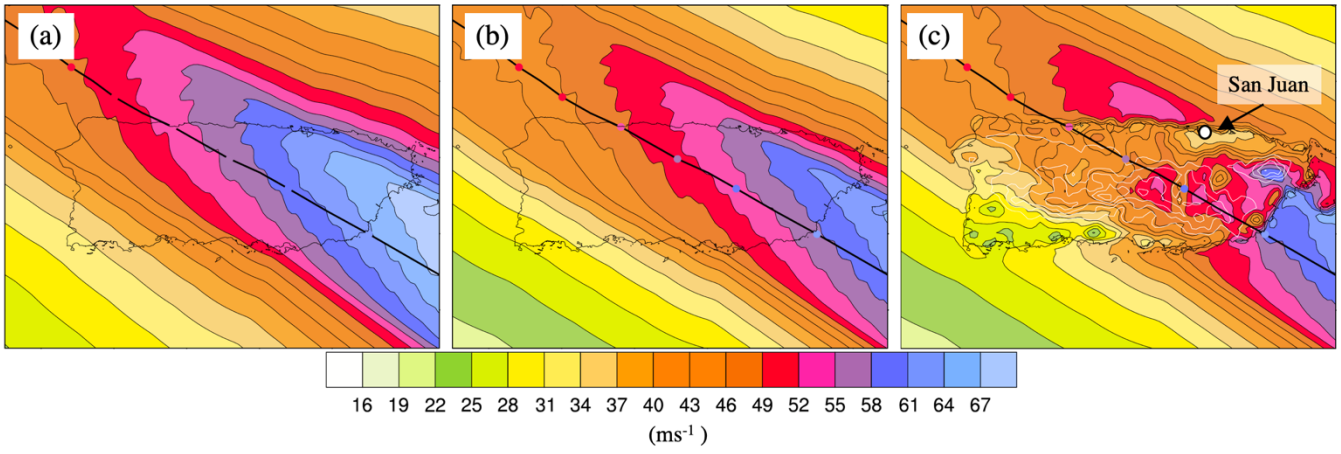

Figure 2: Simulated footprints (ms^{-1}) for the case of Hurricane Maria (2017) over Puerto Rico using a) Willoughby only, b) Willoughby and KW01 and no land, and c) Willoughby and KW01 including land. The hurricane track is shown by the thick black line with input V_{max} shown every 6 hours along the track (coloured dots). Coastlines are shown by the thin black lines, and are only included in a) and b) to aid interpretation. Terrain height is contoured every 200m using white lines in c).

4 Evaluation

Kepert (2012) notes that '*The boundary layer in a tropical cyclone is in some respects unlike that elsewhere in the atmosphere. It is therefore necessary to evaluate boundary layer parameterizations for their suitability for use in tropical cyclone simulation.*' Here we present a model evaluation for a subset of historical landfalling TCs to assess the model's capability to reproduce observed wind speeds.

While reanalysis products provide historical footprints as a convenient gridded product, they themselves are a modelled product that contains various assumptions and inaccuracies. In addition, reanalyses are typically standardised to a given land surface type. The HWIND reanalysis product (Powell et al., 1998), for example, is only valid for open-terrain exposure and therefore commonly exceeds wind values from surface observing stations. We therefore choose to evaluate the model against surface station observations provided by the 3-hourly NMC ADP Global Surface Observations Subsets

https://doi.org/10.5194/nhess-2019-207
Preprint. Discussion started: 2 July 2019


Natural Hazards and Earth System Sciences Discussions

(NCEP/NWS/NOAA/U.S. Department of Commerce). Wind averaging periods were converted from 2-minute to 1-minute for onshore station data and from 10-minute to 1-minute for offshore buoy using the World Meteorological Organization conversion factors in Table 1.1 of Harper et al., (2010).

Since the U.S. has the highest density observing sites, a subset of 8 U.S. landfalling storms was chosen for the evaluation. This subset includes storms making landfall on the Gulf Coast (Rita (2005), Katrina (2005) and Ivan (2004)), Florida (Charley (2004), Irma (2017) and Wilma (2005)), and the U.S. Northeast (Sandy (2012) and Irene (2011)). An example model comparison with observations is shown in Fig. 3 for Hurricane Wilma in Florida. For risk management the accuracy of wind speeds over urban is of critical importance. For the model to be as useful as possible a low wind speed bias over urban areas is corrected in a post-processing step. A bias correction factor of 20% is applied to the wind speeds over urban areas. This factor was determined through the evaluation of the full subset of storms described later in this section. The effect of this correction can be seen over the urban area of Miami for the case of Hurricane Wilma in Fig. 3a

Figure 3a shows the simulated footprint places the strongest winds to the right of track for this fast-moving storm, as expected. The winds weaken abruptly as Wilma makes landfall and the boundary layer model adjusts to the increased surface friction of the land surface. The lack of significant topography over South Florida allows the effect of variable overland surface roughness to be seen. The largest perturbation is the acceleration over the low friction surface of Lake Okeechobee. Finally, the footprint shows the reacceleration of winds as Wilma exits Florida, due to the increasing intensity of Willoughby's gradient wind profile and the reduced surface friction. The strongest footprint winds compare well to the input track winds (compare the coloured contours with the coloured dots along the track line in Fig. 3a). The spatial footprint compares well with the reanalysed HWIND footprint (http://www.hwind.co/legacy_data/, Powell et al., 1998) (compare Figs. 3a and 3b). Both footprints capture similar overland wind speeds and asymmetry. But the footprint captures more small-scale variability such as the over-lake wind speed-up not permitted by the open-terrain exposure assumption of HWIND.

A comparison of the storm lifetime maximum wind speed at the locations of available surface station observations is shown in Fig 3c. Differences between model and observations are mostly within ±8m/s across Florida. The same comparison between HWIND and surface station observations is not shown because the adjustment to open-terrain exposure in HWIND means the observations are not comparable. Figure 3d shows a scatter plot of model versus observed instantaneous 1-minute wind speeds throughout the lifetime of the storm, shown for observed potentially damaging winds (values greater than 18ms^{-1}, equivalently 40mph). Points are shown for all instances of the observation time falling within 3 hours of the model time. While a perfect correspondence between model and observations would lie along the 1-1 line, some scatter is expected due to the relatively coarse model grid not resolving fine-scale variability and the loss in predictability of fine-scale variability. The scatter plot shows no evidence of a substantial bias across the range of storm wind speeds.

https://doi.org/10.5194/nhess-2019-207
Preprint. Discussion started: 2 July 2019

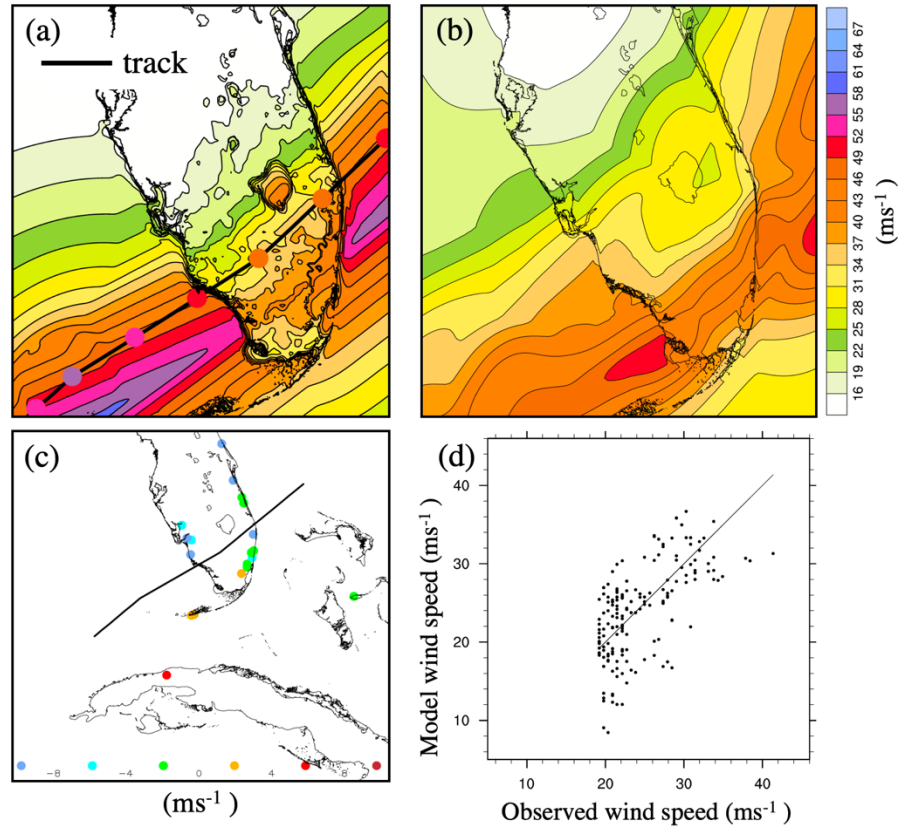

Figure 3: Hurricane Wilma (2005) in a) model footprint (ms^{-1}) including the hurricane track and input track maximum wind speed every 6 hours (coloured dots), b) HWIND footprint (ms^{-1}), c) difference between model and observed storm-lifetime maximum wind speeds at the locations of surface station observations (ms^{-1}), and d) scatter plot of modelled and observed wind speeds showing all station locations that exceeded 18ms^{-1} observed through the lifetime of the storm. All data are the 1-minute sustained wind.

Model performance across the 8 U.S. storms is summarized in Fig. 4. To better understand model performance, the comparison with observations explores model bias as a function of distance from the TC centre, and split by left-of-track and right-of-track. Again, points are shown for all instances of the observed time falling within 3 hours of the model time. Figures 4a and 4b show there is little evidence of large bias with the vast majority of differences falling within ±10m/s. There is also no strong variation in bias with distance from the storm centre. Possible explanations for an apparent low bias within 20km of the storm centre are i) storm centre location error in the input track data, or ii) use of an average value for R_{max}. Our use of this average value was to enable use of readily available data. A next iteration of the model could explore the benefits of adding asymmetry in R_{max}.

The model performs similarly well on both sides of the storm, indicating that our treatment of asymmetry due to translation speed captures a major portion of the observed asymmetry. Considering only urban locations that experienced winds exceeding

https://doi.org/10.5194/nhess-2019-207
Preprint. Discussion started: 2 July 2019

Natural Hazards and Earth System Sciences
Discussions

18ms^{-1} (Figs. 4c and 4d), after applying the 20% bias correction factor the model shows no large bias. While there is a suggestion of a low bias for winds far from the storm centre, the vast majority of points lie within 10ms^{-1} of the observations. The most damaging winds also reside close to R_{max} (in the range 20-100km from the TC centre) where our bias is smallest.

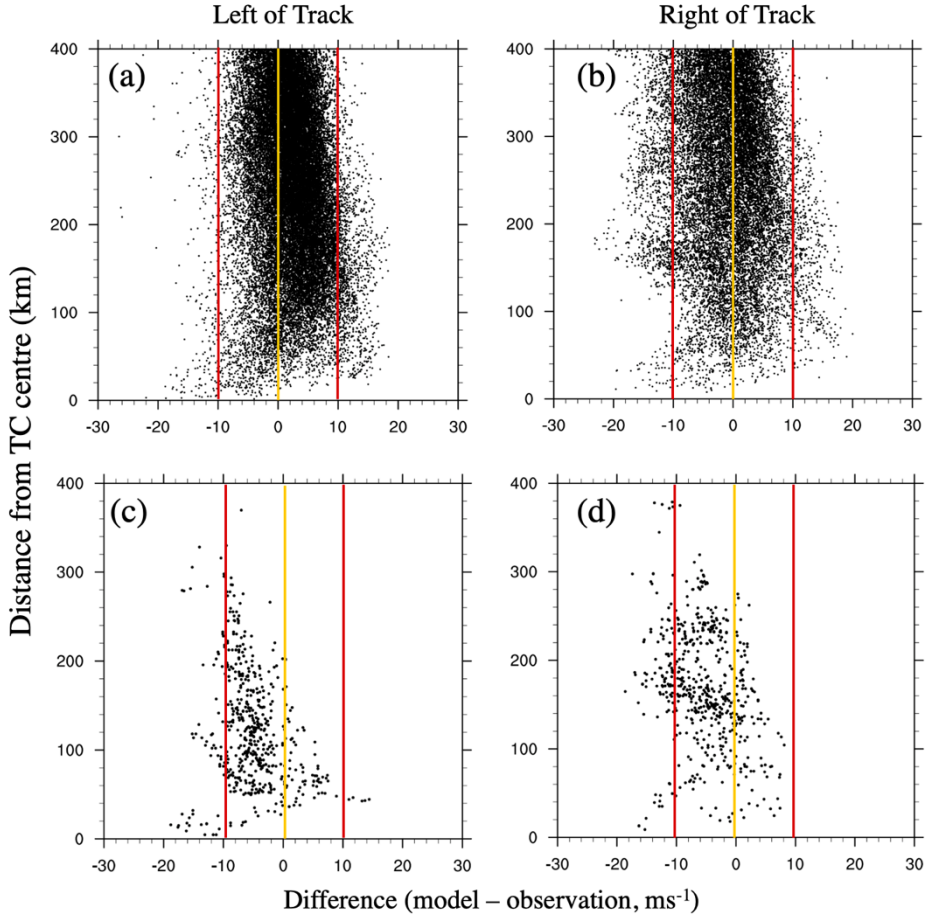

Figure 4: Difference between modelled and observed wind speeds for the 8 U.S. storms as a function of distance from the TC centre (ms^{-1}) and split by left of track (left column) and right of track (right column). The upper row shows all data points, and the lower row shows only urban data points that experienced observed wind speeds greater than 18ms^{-1}. The orange lines indicate zero difference and the red lines indicate a positive and negative difference of 10ms^{-1}.

5. A Dataset of Global Historical Landfalling TC Footprints

One application of the model is demonstrated here through the creation of the dataset of global historical landfalling TC footprints. For global consistency, the input track data source is the global IBTrACS v04 dataset (Knapp et al., 2010). The data record length extends as far back as the required input data are available. Archived R_{max} data extend back to 1988 for the North Atlantic and the East Pacific, but extend back only as far as the early 2000s for the other basins. While Tan and Fang

https://doi.org/10.5194/nhess-2019-207
Preprint. Discussion started: 2 July 2019

Natural Hazards and Earth System Sciences
Discussions

(2018) fill in missing variables using empirical relationships between TC variables, we choose to exclude tracks with missing data. For all basins, landfalling track points are identified using the landfall flag in the IBTrACS dataset (Knapp et al. 2010). Bypassing storms are included to capture the storms that don't make landfall, but still bring strong winds onshore. Such storms are identified using the 'distance to land' variable in IBTrACS, and defined as TCs that track within 50km of a coastline, or within 250km of the coastline with maximum wind speeds greater or equal to 50kts (58mph). Since our interest is in winds over land, storms are simulated from approximately 12 hours before landfall (or before the closest point to land for bypassing storm) as far inland as the end of the track, or until the TC tracks back out over open water.

The final dataset consists of 714 footprints. Figure 5 shows the locations of 17 simulation domains together with the numbers of simulated footprints per domain. Figure 6 shows all tracks simulated for three example domains: The Gulf and Southeast U.S. coast, Eastern China and Taiwan, and Eastern Australia. The numbers and spatial density of tracks vary due to different periods of records for the different basins and the different frequencies of landfalling storms. Each footprint contains the storm lifetime maximum 1-minute average wind at 10 meters above Earth's surface. The units are meters per second. Each footprint is on a latitude longitude grid with a grid spacing between 2- and 4-km depending on the regional domain.

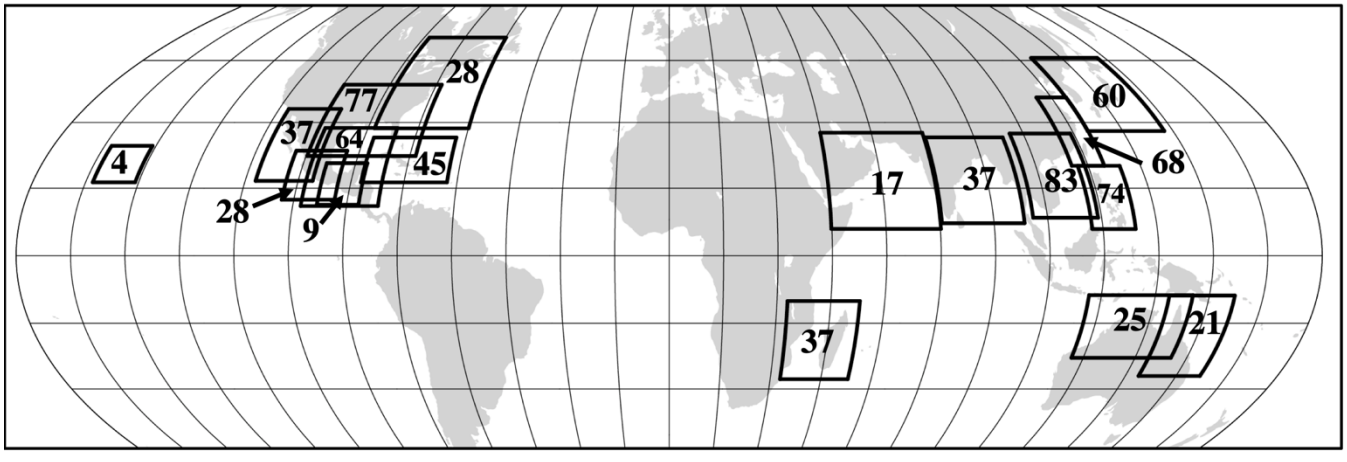

Figure 5: A global map of the 17 simulation domains used in the creation of the dataset of historical global TC footprints. The numbers of simulated footprints for each domain is indicated.

https://doi.org/10.5194/nhess-2019-207
Preprint. Discussion started: 2 July 2019

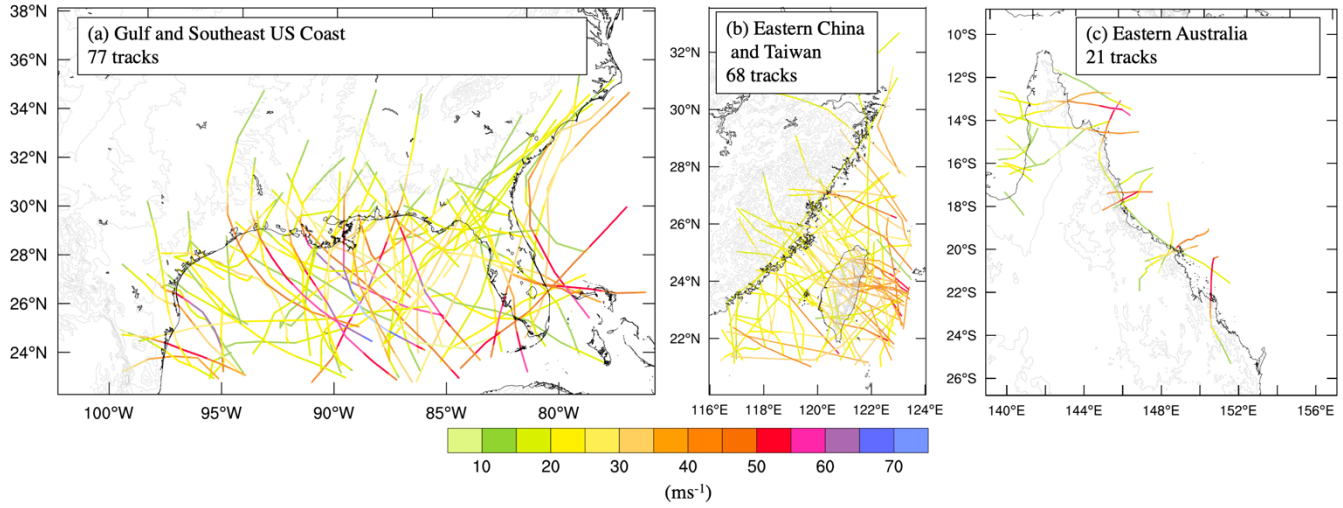

Figure 6: TC tracks used to simulate footprints for domains over a) the Gulf and Southeast U.S. coast, b) Eastern China and Taiwan, and c) Eastern Australia. Tracks are coloured by the track V_{max} (ms^{-1}). Track data are taken from IBTrACS (Knapp et al. 2010).

Tan and Fang (2018) suggest substantial regional variations in the inland extent of strong wind. A preliminary analysis of regional variability in the wind speed decay rates with inland track distance is presented here. Figure 7 shows the regional average distance rate-of-change of storm lifetime maximum wind speed and terrain height with along-track distance from the point of landfall for the Gulf and Southeast U.S. coast, Eastern China and Taiwan, and Eastern Australia (the same regions as shown in Fig. 6). Region average values are calculated over all tracks within each region and all data are smoothed using a 30-km running average. The strength of the smoother was chosen as a balance between the need to smooth noisy wind profiles while retaining the effects of coastlines and terrain. The x-axes (along-track extent) are cut off at the distance inland when only three tracks remain.

For the Gulf and Southeast U.S. region averages are calculated over 77 tracks. We see two regimes of behaviour. The winds strongly decay at the coast as the boundary layer adjusts to the increased surface roughness. The winds then decay more moderately as the tracks extend further inland. The average along-track terrain gradient gradually rises to a peak of 210m at an along-track distance of 550km from the point of landfall and does not appear to substantially affect the inland wind profile. For other regions, however, steeper orography appears to have a large effect on the inland winds.

Figure 7b shows the average along-track winds calculated over 68 tracks. The average landfall wind speed of 29ms^{-1} experiences an abrupt decay at the immediate coast, followed by a modest recovery as the storms pass over the steep windward slopes of Taiwan and mainland China. Increasing along-track terrain height drives enhanced vertical diffusion and vertical advection in the boundary layer model, and enhanced horizontal flow through the 3-dimensional continuity equation. The winds then experience some of the strongest decay rates in the entire dataset on the lee-side. The strong influence of terrain is also seen

https://doi.org/10.5194/nhess-2019-207
Preprint. Discussion started: 2 July 2019

Natural Hazards and Earth System Sciences
Discussions

along the coastal ranges of Eastern Australia. Figure 7c shows three peaks of between 250m and 280m in the average terrain height along 21 tracks within 300km of the average point of landfall. Again, the average landfall wind speed of 28ms^{-1} experiences a strong wind decay at the immediate coast before recovering slightly over the first ridgeline and then strongly decaying on the lee side. The rate of decay lessens over the second and third ridgelines.

This preliminary analysis suggests a strong influence of regional terrain on overland footprints. Further investigation is needed to better quantify the effect and understand the extent to which the full range of terrain effects on TC wind fields are captured by this modelling approach.

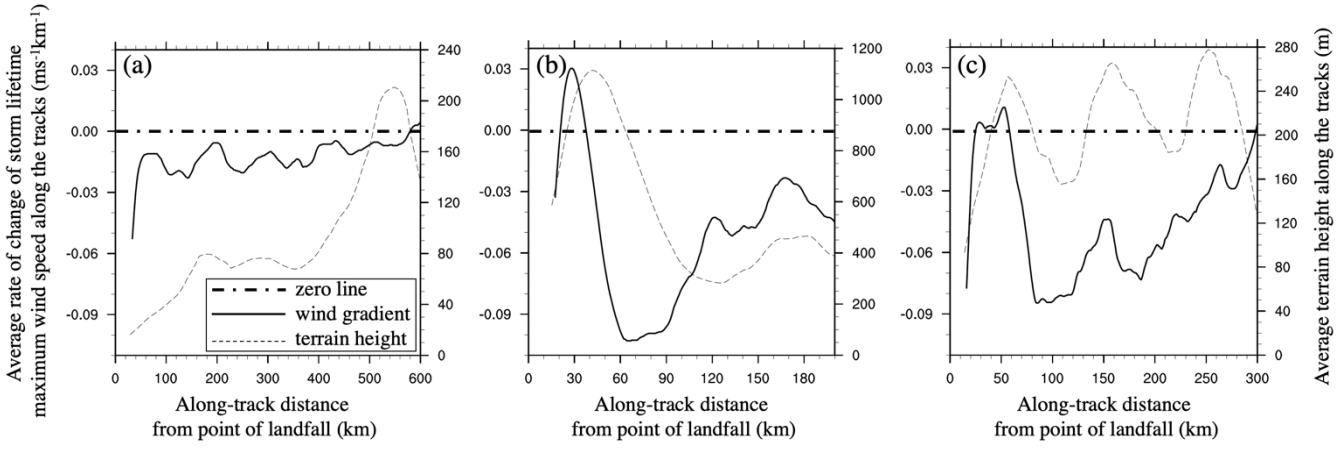

Figure 7: Variation of regional average distance rate-of-change of wind speed (ms^{-1} km^{-1}) and terrain height (m) with along-track distance from the point of landfall (km) for the same regions as shown in Fig. 6; a) Gulf and Southeast U.S. coast, b) Eastern China and Taiwan, and c) Eastern Australia. All data are smoothed using a 30-point running average. Region average values are calculated over all tracks within each region. The x-axes (along-track distance) are cut off at the point where only 3 tracks remain. Each panel has the same left y-axis limits but different right y-axis limits to better show the ranges of regional terrain height.

6. Conclusions

This paper presented a novel and globally-applicable approach to modelling the surface wind field of landfalling TCs. The modelling system simulates the temporal evolution of the near-surface spatial wind fields of landfalling TCs, accounting for terrain effects such as coastlines, inland orography, and abrupt changes in surface friction. A two-step process models the upper wind field using a parametric wind field model fitted to TC track data, then brings the winds down to the surface using a numerical boundary layer model. This represents more of the dynamics and physics of the boundary layer than analytical approaches or empirical wind reduction factors, especially over regions of complex terrain. The guiding principles for model development were to i) use only readily available track data from historical archives, real-time forecasts or synthetic track

https://doi.org/10.5194/nhess-2019-207
Preprint. Discussion started: 2 July 2019


Natural Hazards and Earth System Sciences Discussions

models, and ii) maintain balance between representing the necessary physics of the land surface-flow interactions and the need for computational speed for future applications to probabilistic wind speed assessment.

The model is suitable for simulating the near-surface wind field throughout the entire lifecycle of translating, strengthening/weakening, expanding/contracting, and landfalling TCs. An evaluation of a subset of 8 U.S. landfalling TCs against surface station observations showed that the model had no large bias across all storm radii, and across both sides of the storm tracks. This suggests that the treatment of asymmetry (the addition of a radially-varying fraction of the TC translation vector) captures much of the observed asymmetry. For a case study of Hurricane Maria (2017), the inclusion of variable surface friction and terrain height was shown to add substantial sub-storm scale variability to the footprint. Winds dropped abruptly at the coast, yet accelerated over windward slopes and mountain crests. Winds also decelerated over the high surface drag of urban areas. Further work is needed to verify the extent to which the full terrain and surface drag effects are included in the modelling approach. In addition to a process-level evaluation against observations, the efficacy of the approach could be assessed through comparison with numerical weather prediction model simulations to understand where the approach fails. But differences in TC tracks and vertical model grid spacings would need careful consideration. The overarching aim would be to identify the key terrain effects needed to be included in computationally efficient overland TC wind models.

An application of the model was demonstrated through the creation of a dataset of 714 global historical TC footprints, and is referred to as the Willis Research Network Global Tropical Cyclone Wind Footprint dataset version 1. While previous studies have mapped global historical TC wind fields, none included the full nonlinear adjustments of the surface wind field to variable terrain. This unique dataset is a rich resource to advance our process-level understanding of spatial and temporal variability in overland TC winds. A preliminary analysis showed strong regional variability in the inland extent of damaging surface winds, as controlled by regional TC and terrain characteristics. Analysis of regional average footprints showed acceleration over windward slopes leading to some recovery of the abrupt wind speed reduction at the immediate coast. For risk management, this dataset may be used to better understand historical losses in regions of complex topography, and support the generation of synthetic event sets, particularly in regions of sparse historical data.

Other applications include real-time forecasting of overland TC winds in advance of approaching TCs. The model also may be used to produce wind exceedance probabilities (following a similar approach to Arthur et al., 2008). High efficiency permits large numbers of simulations that could be used as inputs to a Generalized Extreme Value fit to the data to quantify the extremes. Another opportunity presented by this 3-dimensional modelling of the boundary layer wind structure is an assessment of wind loading on high-rise structures. Today's coastal high-rise structures can extend above the surface layer into wind speeds far in excess of those at the surface (Vickery et al., 2009) at heights that are explicitly simulated in the model.

https://doi.org/10.5194/nhess-2019-207
Preprint. Discussion started: 2 July 2019


Natural Hazards and Earth System Sciences Discussions

While the modelling approach captures more of the dynamics and physics of the TC boundary layer than analytical or empirical approaches, it misses a number of potentially important processes. A nonhydrostatic modelling system, for example, would capture more of the orographic effect (Wang, 2007). Perhaps more important is its accounting for only one-way of what is inherently a two-way interaction between the boundary layer and the free troposphere. For example, terrain variations can enhance convergence and trigger deep convection that may feedback on the low-level winds. TC responses to changes in land surface, such as at landfall, can have substantial effects on the whole TC circulations (e.g., Ramsay and Leslie, 2008; Wu, 2001). Another limitation is the use of a parametric TC wind profile model that is not designed to fit wind profiles of extra-tropical transitioning cyclones. During the process of transition, the wind field can become highly asymmetric and develop wind maxima on either side of the cyclone and far from the cyclone centre (e.g., Loridan et al., 2015). This presents a limitation of our modelling approach and may cause substantial errors in the footprints of strongly transitioning TCs over higher latitudes of the U.S. and Japan, for example. Finally, for wind loading and risk management application, an explicit representation of gusts is desirable.

This paper demonstrated the potential benefits of incorporating a physical representation of terrain effects in a computationally inexpensive model of overland TC surface winds. Future work will explore a process-level evaluation of terrain effects to understand cause of the low wind speed bias over urban areas and more generally to evaluate terrain effects in the model. Future work also will assess the value of this modelling technology and global landfalling TC catalogue in risk management decision making contexts.

Author Contribution

JD, GH, IDW, SP and GS designed the investigation. YW led the methodology and software with contributions from JD and MG. MG ran the simulations, formal analysis, visualization and data curation. JD prepared the writing with contributions from all co-authors.

Competing Interests

The authors declare that they have no conflict of interest.

https://doi.org/10.5194/nhess-2019-207
Preprint. Discussion started: 2 July 2019

Natural Hazards and Earth System Sciences Discussions

Data Availability

The Willis Research Network Global Tropical Cyclone Wind Footprint dataset version 1 will be made publicly available on the lead author's GitHub site on 1st May 2020. This time restriction follows terms of the funder, the Willis Research Network.

Acknowledgements

This work was funded by the Willis Research Network. The visit of Dr. Yuqing Wang to NCAR for the boundary layer model setup was partly supported by NCAR Mesoscale and Microscale Meteorology laboratory visitor funds. NCAR is sponsored by the National Science Foundation.

References

Arthur, W.C., Schofield, A., Cechet, R.P. and Sanabria, L.A.: Return period cyclonic wind hazard in the Australian region. In 28th AMS Conference on Hurricanes and Tropical Meteorology, 2008.

Blackadar, A. K.: The vertical distribution of wind and turbulent exchange in a neutral atmosphere. J. Geophys. Research, 67(8), 3095-3102, https://doi.org/10.1029/JZ067i008p03095, 1962.

Chavas, D. R., Reed, K. A. and Knaff, J. A.: Physical understanding of the tropical cyclone wind-pressure relationship. Nature communications, 8(1), p.1360, https://doi.org/10.1038/s41467-017-01546-9, 2017.

Cobb, A. and Done, J. M.: The Use of Global Climate Models for Tropical Cyclone Risk Assessment. In: Collins J., Walsh K. (eds) Hurricanes and Climate Change. Springer, Cham, https://doi.org/10.1007/978-3-319-47594-3_7, 2017.

Danielson, J.J. and Gesch, D.B.: Global multi-resolution terrain elevation data 2010 (GMTED2010) (No. 2011-1073). US Geological Survey, https://doi.org/10.3133/ofr20111073, 2011.

Davis, C. A., Wang, W., Dudhia, J. and Torn, R.: Does increased horizontal resolution Improve hurricane wind forecasts? Weather and Forecasting, 25, 1826-1841, https://doi.org/10.1175/2010WAF2222423.1, 2010.

Demuth, J., DeMaria, M. and Knaff, J. A.: Improvement of advanced microwave sounder unit tropical cyclone intensity and size estimation algorithms. J. Appl. Meteor., 45, 1573-1581, https://doi.org/10.1175/JAM2429.1, 2006.

Elsner, J. B., Kossin, J. P., Jagger, T. H.: The increasing intensity of the strongest tropical cyclones. Nature 455(7209):92-95, https://doi.org/10.1038/nature07234, 2008.

Emanuel, K. A.: Increasing destructiveness of tropical cyclones over the past 30 years. Nature 436:686-688, https://doi.org/10.1038/nature03906, 2005.

Estrada, F., Botzen, W. J. W., and Tol, R. S. J.: Economic losses from US hurricanes consistent with an influence from climate change. Nat. Geosci., 8, 880–4, https://doi.org/10.1038/ngeo2560, 2015.

Galperin, B., Kantha, L. H., Hassid, S,. and Rosati, A.: A Quasi-equilibrium Turbulent Energy Model for Geophysical Flows. J. Atmos. Sci., 45, 55–62, https://doi.org/10.1175/1520-0469(1988)045<0055:AQETEM>2.0.CO;2, 1988.

Garratt, J. R.: Review of Drag Coefficients over Oceans and Continents. Mon. Wea. Rev., 105, 915–929, https://doi.org/10.1175/1520-0493(1977)105<0915:RODCOO>2.0.CO;2, 1977.

Geiger, T., Frieler, K. and Levermann, A.: High-income does not protect against hurricane losses. Environmental Research Letters, 11, 084012, http://dx.doi.org/10.1061/(ASCE)1527-6988, 2016.

Giuliani, G. and Peduzzi, P.: The PREVIEW Global Risk Data Platform: a geoportal to serve and share global data on risk to natural hazards. Natural Hazards and Earth System Science, 11(1), 53-66, https://doi.org/10.5194/nhess-11-53-2011, 2011.

Harper, B.A., Kepert, J.D. and Ginger, J.D.: Guidelines for converting between various wind averaging periods in tropical cyclone conditions. Geneva, Switzerland: WMO, 2010.

Henderson, D., Ginger, J., Leitch, C., Boughton, G. and Falck, D.: Tropical Cyclone Larry: Damage to buildings in the Innisfail area. CTS Tech. Rep. TR51, Cyclone Testing Station, School of Engineering, James Cook University, Townsville, QLD, Australia, 98 pp, 2006.

Hill, K. A. and Lackmann, G. M.: The impact of future climate change on TC intensity and structure: A downscaling approach. Journal of Climate 24(17), 4644–4661, https://doi.org/10.1175/2011JCLI3761.1, 2011.

Holland, G. J., and Bruyère, C.L.: Recent intense hurricane response to global climate change. Climate Dynamics, 42(3-4), 617-627, https://doi.org/10.1007/s00382-013-1713-0, 2014.

Holland, G. J., Belanger, J. I. and Fritz, A.: A revised model for radial profiles of hurricane winds. Monthly Weather Review, 138, 4393-4401, https://doi.org/10.1175/2010MWR3317.1, 2010.

Jakobsen, F. and H. Madsen, H.: Comparison and further development of parametric tropical cyclone models for storm surge modeling. Journal of Wind Engineering, 92, 375-391, https://doi.org/10.1016/j.jweia.2004.01.003, 2004.

Kepert, J. D.: Observed boundary-layer wind structure and balance in the hurricane core. Part I: Hurricane Georges. J. Atmos. Sci., 63, 2169–2193, https://doi.org/10.1175/JAS3745.1, 2006a.

Kepert, J. D.: Observed boundary-layer wind structure and balance in the hurricane core. Part II: Hurricane Mitch. J. Atmos. Sci., 63, 2194–2211, , https://doi.org/10.1175/JAS3746.1, 2006b.

Kepert, J. D.: Choosing a boundary layer parameterization for tropical cyclone modelling. Monthly Weather Review 140, 1427–1445, https://doi.org/10.1175/MWR-D-11-00217.1, 2012.

Kepert, J. D. and Wang, Y.: The Dynamics of Boundary Layer Jets within the Tropical Cyclone Core. Part II: Nonlinear Enhancement. J. Atmos. Sci., 58, 2485–2501, https://doi.org/10.1175/1520-0469(2001)058<2485:TDOBLJ>2.0.CO;2, 2001.

Knapp, K., Kruk, M. C., Levinson, D. H., Diamond, H. J. and Neumann, C. J.: The International Best Track Archive for Climate Stewardship (IBTrACS). Bull. Amer. Meteor. Soc., 91, 363–376, https://doi.org/10.1175/2009BAMS2755.1, 2010.

Loridan, T., Khare, S., Scherer, E., Dixon, M. and Bellone, E.: Parametric modeling of transitioning cyclone wind fields for risk assessment studies in the western North Pacific. J. Appl. Meteor. Climatol., 54, 624–642, https://doi.org/10.1175/JAMC-D-14-0095.1, 2015.

Loridan, T., Crompton, R. P. and Dubossarsky, E.: A Machine Learning Approach to Modeling Tropical Cyclone Wind Field Uncertainty. Mon. Wea. Rev., 145, 3203–3221, https://doi.org/10.1175/MWR-D-16-0429.1, 2017.

Meng, Y., Matsui, M. and Hibi, K.: A numerical study of the wind field in a typhoon boundary layer. Journal of Wind Engineering and Industrial Aerodynamics 67–68: 437–448, https://doi.org/10.1016/S0167-6105(97)00092-5, 1997.

Miller, C., Gibbons, M., Beatty, K. and Boissonnade, A.: Topographic speed-up effects and observed roof damage on Bermuda following Hurricane Fabian (2003). Weather and Forecasting, 28(1), pp.159-174, https://doi.org/10.1175/WAF-D-12-00050.1, 2013.

Mitchell-Wallace, K., Foote, M., Hillier, J. and Jones, M.: Natural catastrophe risk management and modelling: A practitioner's guide. John Wiley & Sons, https://doi.org/10.1002/9781118906057, 2017.

Murakami, H., Wang, Y., Yoshimura, H., Mizuta, R., Sugi, M., Shindo, E., Adachi, Y., Yukimoto, S., Hosaka, M., Kusunoki, S. and Ose, T.: Future changes in tropical cyclone activity projected by the new high-resolution MRI-AGCM. Journal of Climate, 25(9), 3237-3260, https://doi.org/10.1175/JCLI-D-11-00415.1, 2012.

NCEP/NWS/NOAA/U.S. Department of Commerce.: NMC ADP Global Surface Observations Subsets. Research Data Archive at the National Center for Atmospheric Research, Computational and Information Systems Laboratory. https://doi.org/10.5065/BARE-NP34, 1995. Last accessed Feb 1, 2019.

Pielke Jr, R. A., Gratz, J., Landsea, C. W., Collins, D., Saunders, M. A. and Musulin, R.: Normalized hurricane damage in the united states: 1900–2005. Natural Hazards Review, https://doi.org/10.1061/ASCE1527-698820089, 2008.

Powell, M. D. and Houston, S. H.: Surface wind fields of 1995 Hurricanes Erin, Opal, Luis, Marilyn, and Roxanne at landfall. Mon. Wea. Rev., 126, 1259–1273, https://doi.org/10.1175/1520-0493(1998)126<1259:SWFOHE>2.0.CO;2, 1998.

Powell, M. D., Houston, S. H., Amat, L. R. and Morisseau-Leroy, N.: The HRD real-time hurricane wind analysis system. J. Wind Engineer. and Indust. Aerodyn. 77&78, 53-64, https://doi.org/10.1016/S0167-6105(98)00131-7, 1998.

Powell, M. D., Vickery, P. J. and Reinhold, T. A.: Reduced drag coefficient for high wind speeds in tropical cyclones. Nature, 422, 279–283, https://doi.org/10.1038/nature01481, 2003.

Ramsay, H. A. and Leslie, L. M.: The effects of complex terrain on severe landfalling Tropical Cyclone Larry (2006) over northeast Australia. Mon. Wea. Rev., 136, 4334–4354, https://doi.org/10.1175/2008MWR2429.1, 2008.

Ramsay, H. A., Leslie, L. M. and Kepert, J. D.: A high-resolution simulation of asymmetries in severe Southern Hemisphere Tropical Cyclone Larry (2006). Monthly Weather Review, 137(12), 4171-4187, https://doi.org/10.1175/2009MWR2744.1, 2009.

Ranson, M., Kousky, C., Ruth, M., Jantarasami, L., Crimmins, A. and Tarquinio, L.: Tropical and extratropical cyclone damages under climate change. Climatic change, 127(2), 227-241, https://doi.org/10.1007/s10584-014-1255-4, 2014.

Schwendike, J. and Kepert, J. D.: The boundary layer winds in Hurricanes Danielle (1998) and Isabel (2003). Mon. Wea. Rev., 136, 3168–3192, https://doi.org/10.1175/2007MWR2296.1, 2008.

Smith, S. D.: Coefficients for sea surface wind stress, heat flux, and wind profiles as a function of wind speed and temperature. J. Geophys. Res, 93, 15467–15472, https://doi.org/10.1029/JC093iC12p15467, 1988.

Smith, A. and Katz, R.: U.S. Billion-dollar Weather and Climate Disasters: Data Sources, Trends, Accuracy and Biases. Natural Hazards, https://doi.org/10.1007/s11069-013-0566-5, 2013.

Tan, C. and Fang, W.: Mapping the wind hazard of global tropical cyclones with parametric wind field models by considering the effects of local factors. International Journal of Disaster Risk Science, 9(1), 86-99, https://doi.org/10.1007/s13753-018-0161-1, 2018.

Vickery, P. J., Masters, F. J., Powell, M. D. and Wadhera, D.: Hurricane hazard modeling: The past, present, and future. Journal of Wind Engineering and Industrial Aerodynamics, 97(7-8), 392-405, https://doi.org/10.1016/j.jweia.2009.05.005, 2009.

Villarini, G., and Vecchi, G. A.: Projected increases in North Atlantic tropical cyclone intensity from CMIP5 models. Journal of Climate 26(10), 3231-3240, https://doi.org/10.1175/JCLI-D-12-00441.1, 2013.

Walsh, K. J., McBride, J. L., Klotzbach, P. J., Balachandran, S., Camargo, S. J., Holland, G., Knutson, T. R., Kossin, J. P., Lee, T. C., Sobel, A. and Sugi, M.: Tropical cyclones and climate change. Wiley Interdisciplinary Reviews: Climate Change, 7(1), 65-89, https://doi.org/10.1038/ngeo779, 2016.

Wang, Y.: A multiply nested, movable mesh, fully compressible, nonhydrostatic tropical cyclone model – TCM4: Model description and development of asymmetries without explicit asymmetric forcing. Meteor. Atmos. Phys., 97, 93-116, https://doi.org/10.1007/s00703-006-0246-z, 2007.

Weinkle, J., Maue, R. and Pielke Jr, R.: Historical global tropical cyclone landfalls. Journal of Climate. 25(13), 4729–4735, https://doi.org/10.1175/JCLI-D-11-00719.1, 2012.

Wu, C. C.: Numerical simulation of Typhoon Gladys (1994) and its interaction with Taiwan terrain using the GFDL hurricane model. Mon. Wea. Rev., 129, 1533–1549, https://doi.org/10.1175/1520-0493(2001)129<1533:NSOTGA>2.0.CO;2, 2001.

Youngman, B.D. and Stephenson, D. B.: A geostatistical extreme-value framework for fast simulation of natural hazard events, Proceedings of the Royal Society A: Mathematical, Physical and Engineering Sciences, volume 472, no. 2189, https://doi.org/10.1098/rspa.2015.0855, 2016.

Zhang, J.A., Rogers, R.F., Nolan, D.S. and Marks Jr, F.D.: On the characteristic height scales of the hurricane boundary layer. Monthly Weather Review, 139(8), 2523-2535, https://doi.org/10.1175/MWR-D-10-05017.1, 2011.